Korean J. Chem. Eng., **30**(4), 831-835 (2013)
DOI: 10.1007/s11814-012-0203-0

Nonlinear numerical simulation on the onset of Soret-driven motion in a silica nanoparticles suspension

Min Chan Kim†

Department of Chemical Engineering, Jeju National University, Jeju 690-756, Korea
(*Received 4 October 2012 • accepted 16 November 2012*)

Abstract−The onset of buoyancy-driven convection in an initially quiescent, horizontal silica nanoparticle suspension layer heated from above is analyzed theoretically. In this thermally-stably stratified fluid layer the Soret diffusion can induce buoyancy-driven motion for the case of the negative separation ratio. For the high Rayleigh number the convective motion sets in during the transient diffusion stage and the onset time of this motion is analyzed by employing the nonlinear numerical simulation. It is interesting that the convective motion is very weak and the diffusional process is dominant even after the onset time of convection, τ_c, and the nonlinear effects are manifested from the time τ_m ($>\tau_c$). The present τ_m explains the existing experimental results quite well.

Key words: Soret-driven Convection, Silica Nanoparticles Suspension, Nonlinear Analysis, Numerical Simulation

INTRODUCTION

Thermal convection in binary mixtures like ethanol-water and ^{3}He-^{4}He or various gas mixtures shows quite different characteristics from that in pure fluids [1-4]. If the suspension of nanoparticles is considered, the spatiotemporal properties of convection are much more complex than those of pure fluids or molecular solutions due to the influence of thermal diffusion, i.e., Soret-induced concentration gradients and also the extremely small particle mobility which can be reflected by the Lewis number Le≤10^{-4}. Here Le (=D_C/α) is the Lewis number, D_C the diffusion coefficient, the thermal diffusivity, respectively. The relative importance of the Soret effect with respect to weak solutal diffusion is measured by the separation ratio ψ(=$(\beta_C/\beta_T)(D_T/D_C)$), where D_T is the Soret diffusion coefficient, D_C is the diffusion coefficient, and β_T(=$-\rho^{-1}(\partial\rho/\partial T)$) and are the thermal and the solutal expansion coefficient, respectively. Here ρ is the density of the fluid.

For non-vanishing ψ, the external temperature gradient induces concentration variations and these create the buoyancy force. Depending on the sign of the separation ratio ψ, the solutal buoyancy force may act in the same direction as the thermal buoyancy force (for the case of positive ψ) but it counteracts this force for the case of negative ψ. For the case of negative ψ Soret effects can induce buoyancy-driven motion even in initially uniform concentration and thermally stable configuration. For the fully-developed linear temperature field the critical Rayleigh number to represent the convective instability is Ra_c=720(Le/ψ) for the linear concentration field, considering the relative time scale of mass diffusion with respect to thermal diffusion [5].

In the present study the onset of Soret-driven convection in the horizontal nanoparticles suspension layer heated from above with Ra(Le/ψ)$^{-1}$>720, is investigated by employing nonlinear numerical simulation. And, our predictions will also be compared with available experimental results [6-8] and the previous theoretical predictions [9-11].

†To whom correspondence should be addressed.
E-mail: mckim@cheju.ac.kr

THEORETICAL ANALYSIS

1. Governing Equations

The problem considered here is a horizontal fluid layer confined between two rigid plates separated by the vertical distance d. The schematic diagram of the basic system of pure diffusion is shown in Fig. 1. The fluid layer, of which ψ has a large negative value, is initially quiescent at a constant concentration C_0 and a constant temperature T_0. For time t≥0 the fluid layer is heated suddenly from above with a constant temperature T_1. For the case of Ra(Le/ψ)$^{-1}$> 20, buoyancy-driven convection will set in at a certain time and the governing equations of motion, temperature and concentration fields are expressed by employing the Boussinesq approximation [12]:

$$\nabla\cdot\mathbf{u}=0, \tag{1}$$

$$\frac{\mathrm{Le}}{\mathrm{Pr}}\left\{\frac{\partial}{\partial\tau}+\mathbf{u}\cdot\nabla\right\}\mathbf{u}=-\frac{\mathrm{Le}}{\mathrm{Pr}}\nabla\mathrm{p}+\nabla^2\mathbf{u}-\mathrm{Ra}_S\left(\mathrm{c}+\frac{1}{\psi}\theta\right)\mathbf{k}, \tag{2}$$

$$\left\{\frac{\partial}{\partial\tau}+\mathbf{u}\cdot\nabla\right\}\theta=\frac{1}{\mathrm{Le}}\nabla^2\theta, \tag{3}$$

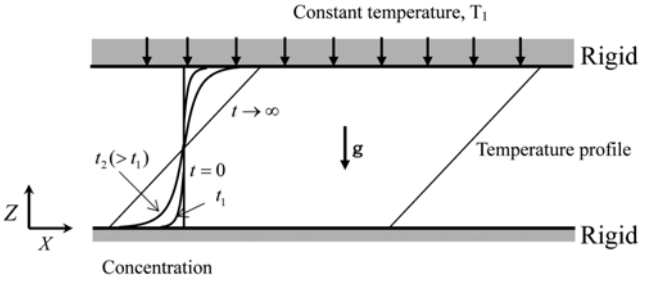

Fig. 1. Schematic diagram of the basic diffusion state considered here.

$$\left\{\frac{\partial}{\partial\tau}+\mathbf{u}\cdot\nabla\right\}c=\nabla^2(c-\theta), \tag{4}$$

where $\mathbf{u}$(=u, v, w) is dimensionless velocity vector, Pr(=ν/α) the Prandtl number, τ the dimensionless time, p the dimensionless pressure, c the dimensionless concentration, θ the dimensionless temperature, Ra_S=Ra(Le/ψ)$^{-1}$ and Ra=g$\beta\Delta Td^3/(\alpha\nu)$, where ν is the kinematic viscosity. We scale lengths by the depth d of the layer, times by the vertical diffusion time d^2/D_C, velocities by D_C/d and accordingly pressure field by $\rho D_C/d^2$. The temperature deviation from its initial distribution ($T-T_0$) and that of concentration field ($C-C_0$) are scaled by $\Delta T(=T_0-T_1)$ and $-\Delta T(D_T/D_C)$, respectively.

We use the following no-slip boundary conditions for the velocity field, perfect heat conduction conditions for the temperature field and impermeable for the concentration field at the top and bottom plates,

$$\mathbf{u}=0,\ \theta=0,\ \frac{\partial}{\partial z}(c-\theta)=0\ \text{ at }\ z=0, \tag{5a}$$

$$\mathbf{u}=0,\ \theta=1,\ \frac{\partial}{\partial z}(c-\theta)=0\ \text{ at }\ z=1. \tag{5b}$$

The present system is thermally stable due to the heating from above, *i.e.* $T_1>T_0$ and therefore Ra<0.

For the limiting case of small Le, the governing equations of flow and concentration fields are reduced as

$$\nabla\cdot\mathbf{u}=0, \tag{1}$$

$$\frac{Le}{Pr}\left\{\frac{\partial}{\partial\tau}+\mathbf{u}\cdot\nabla\right\}\mathbf{u}=-\frac{Le}{Pr}\nabla p+\nabla^2\mathbf{u}-Ra_S\left(c+\frac{z}{\psi}\right)\mathbf{k}, \tag{6}$$

$$\left\{\frac{\partial}{\partial\tau}+\mathbf{u}\cdot\nabla\right\}c=\nabla^2 c, \tag{7}$$

where the temperature field is assumed θ=z [9-11]. The proper boundary conditions are

$$\mathbf{u}=0\ \text{ and }\ \frac{\partial c}{\partial z}=1\ \text{ at }\ z=0\ \text{ and }\ z=1. \tag{8}$$

At steady state the basic temperature and concentration profiles are linear and time-independent, and its critical condition is well summarized by Ryskin et al. [5]. However, for the case of Ra(Le/ψ)$^{-1}$>720 convective motion can occur during the transient diffusion process and the related stability problem becomes transient. For a certain Rayleigh number of Ra_S>720, buoyancy-driven convection will set in at a certain time. For $Ra_S\geq 720$ the velocity and concentration fields are decomposed into the horizontal mean and its fluctuations:

$$\begin{Bmatrix}\mathbf{u}\\ c\end{Bmatrix}=\begin{Bmatrix}\bar{\mathbf{u}}\\ \bar{c}\end{Bmatrix}+\begin{Bmatrix}\mathbf{u}'\\ c'\end{Bmatrix}, \tag{9}$$

where the fluctuations are the function of τ, x, y and z.

To examine the temporal behaviors of thermal instabilities, the following temporal growth rates of the mean value and its fluctuations are defined as

$$\sigma_0=\frac{1}{E_0^{1/2}}\frac{dE_0^{1/2}}{d\tau}\ \text{ and }\ \sigma_1=\frac{1}{E_1^{1/2}}\frac{dE_1^{1/2}}{d\tau}, \tag{10}$$

where $E_0=\int_\Omega \bar{c}^2 d\Omega$ and $E_1=\int_\Omega c'^2 d\Omega$. With $\sigma_0>\sigma_1$, concentration fluctuations are expected to be several orders of magnitude smaller than that of the mean concentration. Here it is assumed that the system is unstable only when the concentration fluctuations are growing faster than the mean concentration. With $\sigma_1>\sigma_0$, the fluctuations will grow to a measurable magnitude. Therefore, the new stability criteria are suggested as [13,14]

$$\sigma_1=\sigma_0\ \text{ at }\ \tau=\tau_c, \tag{11}$$

which marks the onset condition of intrinsic instability at the earliest time τ_c by the critical dimensionless wave number. With an increase in Ra_S it is evident that $\sigma_0\to 3/(4\tau)$ as $\tau\to 0$, and during $\tau_c\leq\tau\leq\tau_m$, $\sigma_1>\sigma_0$. Here τ_m is the time when σ_1 reaches its maximum value. The fastest growing mode of instability is that to reach $\sigma_1=\sigma_0$ at the earliest time τ_c. Therefore, the intrinsic instability is defined as a fastest growing mode subjected to Eq. (11).

For 2-dimensional rolls of a_x=a and a_y=0, the dimensionless governing equations can be expressed as

$$\frac{\partial u}{\partial x}+\frac{\partial w}{\partial z}=0, \tag{12}$$

$$\frac{Le}{Pr}\left\{\frac{\partial}{\partial\tau}+u\frac{\partial}{\partial x}+w\frac{\partial}{\partial z}\right\}u=-\frac{Le}{Pr}\frac{\partial p}{\partial x}+\left(\frac{\partial^2}{\partial x^2}+\frac{\partial^2}{\partial z^2}\right)u, \tag{13}$$

$$\frac{Le}{Pr}\left\{\frac{\partial}{\partial\tau}+u\frac{\partial}{\partial x}+w\frac{\partial}{\partial z}\right\}w=-\frac{Le}{Pr}\frac{\partial p}{\partial z}+\left(\frac{\partial^2}{\partial x^2}+\frac{\partial^2}{\partial z^2}\right)w-Ra_S\left(c+\frac{z}{\psi}\right), \tag{14}$$

$$\left\{\frac{\partial}{\partial\tau}+u\frac{\partial}{\partial x}+w\frac{\partial}{\partial z}\right\}c=\left(\frac{\partial^2}{\partial x^2}+\frac{\partial^2}{\partial z^2}\right)c, \tag{15}$$

under the following boundary conditions:

$$u=w=\frac{\partial c}{\partial z}-1=0\ \text{ at }\ z=0, \tag{16a}$$

$$u=w=\frac{\partial c}{\partial z}-1=0\ \text{ at }\ z=1, \tag{16b}$$

$$\frac{\partial u}{\partial x}=\frac{\partial w}{\partial x}=\frac{\partial\theta}{\partial x}=0\ \text{ at }\ x=-\frac{\pi}{a}\ \text{ and }\ \frac{\pi}{a}. \tag{16c}$$

Here, only the single mode convection having the wavelength 2π/a is considered.

The above equations are here solved numerically with the proper initial conditions. However, we do not know what initial conditions exist at τ=0. The selection of the proper initial conditions is a complex question. From the dominant mode solution [10], it is possible to construct a concentration field at the excitation time $\tau=\tau_i$ as

$$\bar{c}=\sqrt{4\tau_i}\left\{-\text{ierfc}\left(\frac{z}{2\sqrt{\tau_i}}\right)+\text{ierfc}\left(\frac{1-z}{2\sqrt{\tau_i}}\right)\right\}, \tag{17a}$$

$$c'=\varepsilon\left\{\exp\left(-\frac{z^2}{4\tau_i}\right)+\exp\left(-\frac{(1-z)^2}{4\tau_i}\right)\right\}\cos(ax), \tag{17b}$$

where ε is the magnitude of the concentration fluctuation at $\tau=\tau_i$. Here τ_i and ε ought to be small values, and $\varepsilon/\sqrt{\tau_i}\ll 1$ should be satisfied since $|c'/\bar{c}|\ll 1$. In the present study, $Ra_S^{1/2}\tau_i$=0.1 and $\varepsilon Ra_S^{1/4}$=0.01 were set. The relation of $|w/c'|\propto\tau$ for $\tau\to 0$ can be obtained from the dominant mode method [10], *i.e.*, the magnitude of velocity fields is much smaller than the concentration fluctuation; $u(\tau_i)=w(\tau_i)\to 0$ was assumed here.

2. Solution Method

The governing Eqs. (12)-(15) were discretized by an implicit finite-volume, finite-difference based method. For the numerical solution an open source code was adopted [15], where the SIMPLE algorithm [16] with collocated-variables arrangement was applied to calculate pressure. For the stabilization of pressure-velocity coupling, the interpolated cell face velocities were modified by the difference between the interpolated pressure gradient and the gradient calculated at the cell face. The system of linear equations was solved by using Stone's strongly implicit procedure. The time derivatives were discretized by a forward difference scheme. The convection terms were treated by the second-order central difference scheme. For details describing the full algorithm we refer to Ferziger and Peric [15]. Time marching with fixed time step was used. The maximal number of outer iterations per each time step was equal to 1000, allowing to reach residuals of less than 10^{-9}. Grid-convergence and time-step-convergence tests were conducted by repeating calculation for several grids and time-steps. We used a grid of at least 100×200 along the x- and z-directions and the time step less than 10^{-4}.

RESULTS AND DISCUSSION

For the silica nanoparticles suspension of which Le=1.48×10^{-4}, $\Psi=-3.41$ and Pr=5.5 [8], the typical σ_0- and σ_1-curves of two-dimensional rolls are shown with time in Fig. 2. As shown in this figure, for the case of $Ra_S=10^{10}$ the disturbance with the critical wave number of $a_c=85$ grows more rapidly than any other disturbances and reaches $\sigma_0=\sigma_1$ at $\tau=\tau_c$. For $Ra_S=10^8$-10^{10}, the numerical results of σ_0 and σ_1 are summarized in Fig. 3. This figure suggests that $\tau Ra_S^{1/2}$ is a proper time scale and the relation of $\tau_c Ra_S^{1/2}$~constant can be assumed for the limiting case for $Ra_S\rightarrow\infty$.

Under linear stability theory, the critical conditions have been predicted using various methods such as propagation theory [9], dominant mode method [10] and quasi-steady state approximation [11]. These theoretical predictions are compared with the present ones in Fig. 4. For $Ra_S\geq10^6$, the critical conditions based on the present simulations can be summarized as

$$\tau_c Ra_S^{1/2}=5.82 \text{ and } a_c Ra_S^{-1/4}=0.27. \quad (18)$$

These predictions are quite similar to those obtained as the propa-

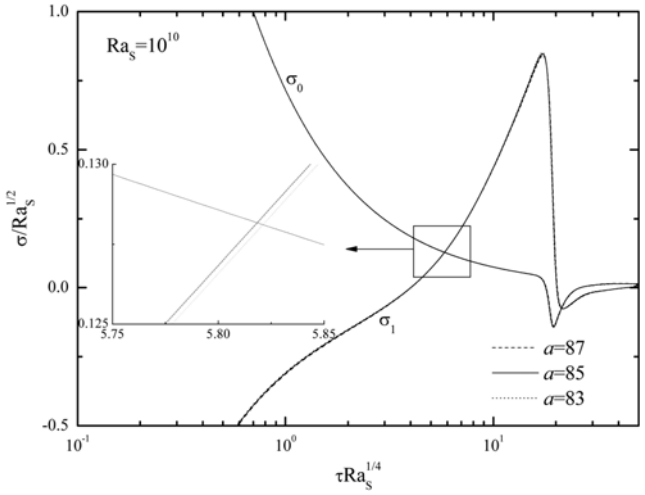

Fig. 2. Growth rates with time at $Ra_S=10^{10}$ for various wave numbers.

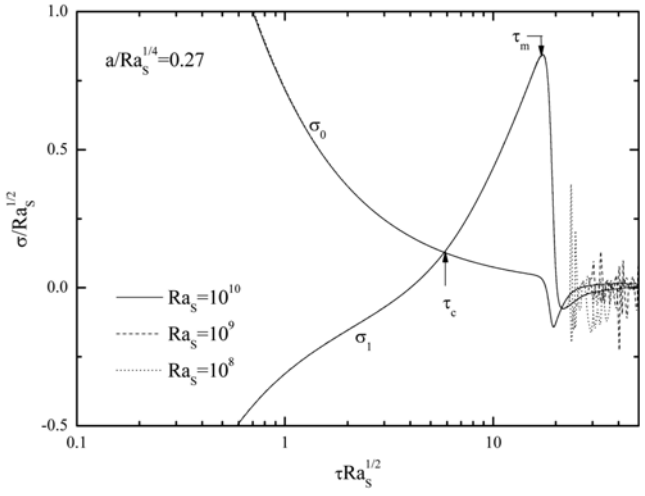

Fig. 3. Growth rates with time at $a/Ra_S^{1/4}$ for the various Ra_S.

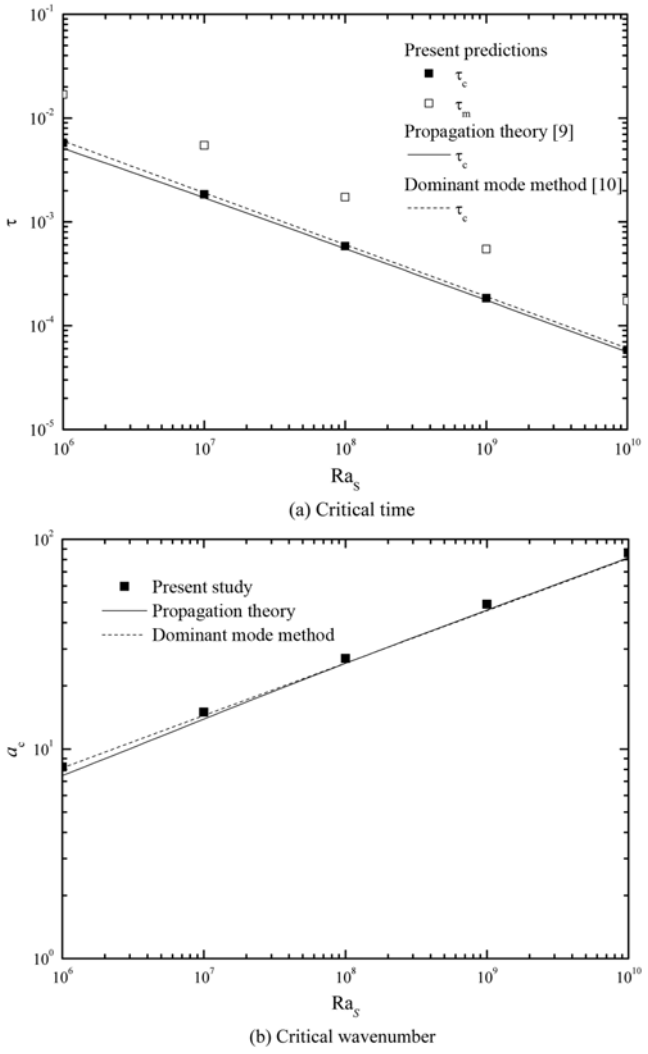

Fig. 4. Comparison of present theoretical predictions with previous one. (a) critical time and (b) critical wavenumber.

gation theory [9], the dominant mode method [10] and the quasi-steady state approximation [11], *i.e.* $\tau_c Ra_S^{1/2}$=5.82, 6.03 and 5.58, and $a_c Ra_S^{-1/4}$=0.26, 0.25 and 0.26, respectively. Furthermore, for the present initiation conditions described below the Eq. (17), the following relation can be obtained:

$$\tau_m Ra_S^{1/2}=17.29. \quad (19)$$

By using the shadowgraph method Mazzoni et al. [8] and Cerbino et al. [17] visualized the Soret-driven convective motion in a colloidal suspension of 22 nm diameter silica particles (LUDOX®) dispersed in water. They obtained the latency time τ^* and the peak time τ_p as the characteristic times when the variance of the intensity of images starts to grow, and it shows the maximum value, respectively. They also measured the oscillation period τ_{osc} as a function of Ra_S. These experimental data are compared in Fig. 5. As shown in this figure, our τ_m-values bound the experimental τ^*-values quite well. As expected, the peak time τ_p is a little larger than the latency time τ^*. Interestingly, our τ_m-values are also close to the oscillation period τ_{osc}. The present τ_m with $Ra_S^{1/2}\tau_i$=0.1 and $\varepsilon Ra_S^{1/4}$=0.01 predicts the experimental data quite well, as shown in Fig. 5(b). For $\tau_c \le \tau \le \tau_m$ fluctuations grow superexponentially and therefore, they are exhibited clearly near $\tau=\tau_m$. For $\tau>\tau_m$, multimode disturbances are possible and the present single-mode disturbance will compete with them and finally transition to turbulent convection.

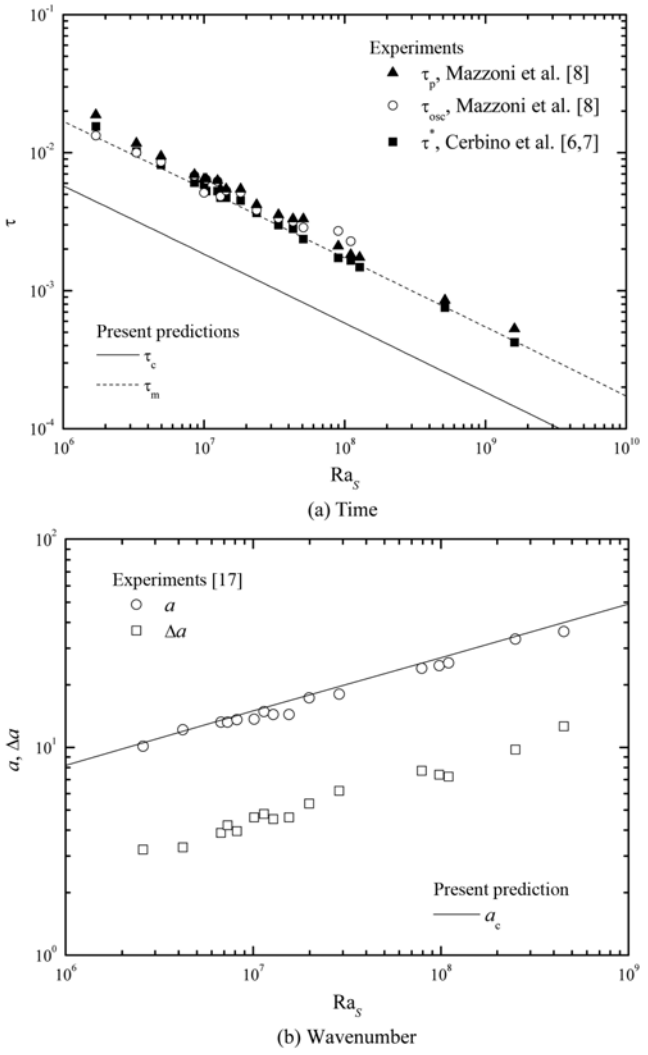

Fig. 5. Comparison of characteristic times and wavenumbers with available experimental data. (a) time and (b) wavenumber.

Giavazzi and Vailati [18] determined the wavenumber at the onset of convection by processing the shadowgraph images. They fitted their spectral profile with a Gaussian function of the form $G(a)=A\exp\{-(a-\bar{a})^2/(2\Delta a)^2\}$, where $\bar{a}$ and Δa represent the dimensionless peak position and width, respectively. They fitted their data $\bar{a}=(0.3\pm0.1)Ra_s^{0.24\pm0.02}$ and $\Delta a=(0.1\pm0.05)Ra_s^{0.25\pm0.02}$. As shown in Fig. 5(b), the present a_c explains their experimental data quite well.

CONCLUSION

The critical condition to mark the onset of convective motion in silica nanoparticle-water suspension heated from above has been analyzed based on the nonlinear numerical simulation. Based on the results of linear stability theory, the growth of the single mode disturbance is traced by employing numerical simulation. The critical times τ_c obtained from the previous linear theory and the present single mode nonlinear disturbance dynamics support each another. From the present calculation and the previous experimental results, the time τ_m to mark first visible motion explains the experimental τ^*-values quite well. In the present silica nanoparticle system, $\tau Ra_S^{1/2}$ seems to be a proper time scale.

ACKNOWLEDGEMENT

This work was supported by the National Research Foundation of Korea Grant funded by the Korean Government (NRF-2010-013-D00014).

NOMENCLATURE

a : dimensionless wavenumber
C : concentration
c_0 : dimensionless base concentration, $D_C(C-C_0)/(j_S d)$
d : distance between the plates
D_C : diffusion coefficient
D_T : Soret diffusion coefficient
g : gravitational acceleration
Le : Lewis number, D_C/α
P : pressure
Pr : Prandtl number, ν/α
Ra : Rayleigh number, $g\beta_T\Delta T d^3/\alpha\nu$
Ra_S : Rayleigh number based on Soret flux, $Ra(Le/\psi)^{-1}$
T : temperature
t : time
(U, V, W) : velocities in Cartesian coordinates
(u, v, w) : dimensionless velocity disturbances in Cartesian coordinates
(X, Y, Z) : Cartesian coordinates
(x, y, z) : dimensionless Cartesian coordinates

Greek Symbols

α : thermal diffusivity
β_C : solutal expansion coefficient, $(1/\rho)(\partial\rho/\partial C)$

β_T : thermal expansion coefficient, $(-1/\rho)(\partial\rho/\partial T)$
θ_0 : dimensionless base temperature, $(T_i - T)/\Delta T$
ν : kinematic viscosity
ρ : density
σ : growth rate
τ : dimensionless time, $D_C t/d^2$
ψ : separation ratio, $(\beta_C/\beta_T)(D_T/D_C)$

Subscripts

c : critical conditions
i : initial conditions
0 : basic quantities
1 : perturbed quantities

REFERENCES

1. G. Ahlers and I. Rehberg, *Phys. Rev. Lett.*, **56**, 1373 (1986).
2. E. Moses and V. Steinberg, *Phys. Rev. Lett.*, **57**, 2018 (1986).
3. J. Liu and G. Ahlers, *Phys. Rev. E*, **55**, 6950 (1997).
4. A. La Porta and C. M. Surko, *Phys. Rev. Lett.*, **80**, 3759 (1998).
5. A. Ryskin, H. W. Muller and H. Pleiner, *Phys. Rev. E*, **67**, 046302 (2003).
6. R. Cerbino, A. Vailati and M. Giglio *Phys. Rev. E*, **66**, 055301(R) (2002).
7. R. Cerbino, A. Vailati and M. Giglio, *Philos. Mag.*, **83**, 2023 (2003).
8. S. Mazzoni, R. Cerbino, D. Brogioli, A. Vailati and M. Giglio, *Eur. Phys. J. E*, **15**, 305 (2004).
9. M. C. Kim, J. S. Hong and C. K. Choi, *AIChE J.*, **52**, 2333 (2006).
10. M. C. Kim, L. H. Kim and D. Y. Yoon, *Korean J. Chem. Eng.*, **26**, 354 (2009).
11. M. C. Kim, *Eur. Phys. J. E*, **34**, 27 (2011).
12. St. Hollingert, M. Lucke and H. W. Muller, *Phys. Rev. E*, **57**, 4250 (1998).
13. J.-C. Chen, G. P. Neitzel and D. F. Jankowski, *Phys. Fluids*, **28**, 749 (1985).
14. M. C. Kim, *Korean J. Chem. Eng.*, **29**, 1688 (2012).
15. J. H. Ferziger and M. Peric, *Computational methods for fluid dynamics*, 2nd Ed., Springer (2002).
16. S. V. Patankar, *Numerical heat transfer and fluid flow*, Hemisphere Pub. Co. (1980).
17. R. Cerbino, A. Vailati and M. Giglio. *Phys. Rev. Lett.*, **94**, 064501 (2005).
18. F. Giavazzi and A. Vailati, *Phys. Rev. E*, **80**, 015303(R) (2009).